

Stabilization of the Electronic Structure at the Cathode/Electrolyte Interface via MgO Ultra-thin Layer during Lithium-ions Insertion/Extraction

Kentaro YAMAMOTO,^a Yuki ORIKASA,^{a, *} Daiko TAKAMATSU,^b Yukinori KOYAMA,^b Shinichiro MORI,^a Titus MASESE,^a Takuya MORI,^a Taketoshi MINATO,^b Hajime TANIDA,^b Tomoya URUGA,^c Zempachi OGUMI^b, and Yoshiharu UCHIMOTO^a

^aGraduate School of Human and Environmental Studies, Kyoto University, Yoshida-nihonmatsu-cho, Sakyo-ku, Kyoto 606-8501 Japan

^bOffice of Society-Academia Collaboration for Innovation, Kyoto University, Gokasho Uji, Kyoto 611-0011, Japan

^cJapan Synchrotron Radiation Research Institute, 1-1-1 Kouto, Sayo-cho, Sayo-gun, Hyogo 679-5198, Japan

Corresponding Author

*Yuki Orikasa

E-mail ; orikasa.yuuki.2a@kyoto-u.ac.jp

TEL : +81-75-753-6850

FAX : +81-75-753-6850

Abstract

Degradation mechanism of surface coating effects at the cathode / electrolyte interface is investigated using thin-film model electrodes combined with *operando* X-ray absorption spectroscopy (XAS). MgO-coated LiCoO₂ thin-film electrodes prepared via pulsed laser deposition at room temperature and high temperature are used as model systems. The MgO coating improves the durability of the cathode during high-potential cycling. *Operando* total reflection fluorescence XAS reveals that initial deterioration due to reduction of Co ions at the surface of the uncoated-LiCoO₂ thin film upon electrolyte immersion is inhibited by the MgO coating. *Operando* depth-resolved XAS reveals that the MgO coating suppresses drastic distortions of local structure at the LiCoO₂ surface as observed in the uncoated-LiCoO₂ during charging process. The electronic and local structure changes at the electrode/electrolyte interface for two types of surface coating morphologies are discussed.

KEYWORDS

Lithium ion battery, surface coating, interfacial structure, *operando* measurement

1. Introduction

Lithium-ion batteries (LIBs) are used in several applications such as mobile phones and electric vehicles, and further improvement of the battery performance is needed. For the improvement of the performance, it is necessary to control the interfacial structure between electrode and electrolyte because the electrode/electrolyte interface is the reaction site of LIBs.¹⁻⁴ One of the popular methods to control the interfacial structure is to coat active materials with a metal oxide.⁵⁻¹² The surface coating of the active materials enhances various aspects of battery performance such as cyclability,⁵⁻⁷ rate capability^{8,9} and durability at high potential.¹⁰⁻¹² However, to the best of our knowledge, the interfacial structure between the electrode and electrolyte upon surface coating is still unclear, particularly when it comes to *in operando* battery operations. This is because direct observation of the interfacial structure is quite difficult. Measurement techniques for the interface with spatial resolution in a nanometric scale under battery operating conditions are required.

Surface X-ray diffraction and X-ray reflectivity measurements have been reported as effective tools to probe interfacial structures under operating conditions of a battery.^{13,14} Although these methods are potent to probe the interface, they however cannot probe amorphous structures or even electronic structural changes. Recently we have developed *operando* total-reflection fluorescence X-ray absorption spectroscopy (TRF-XAS)^{15,16} and *operando* depth-resolved X-ray absorption spectroscopy (DR-XAS).^{17,18} TRF-XAS provides surface-sensitive information regarding the electronic structure at the electrode/electrolyte interface.^{15,16} DR-XAS provides information about the electronic and local structures from the surface to the bulk at a nanometric resolution.^{17,18} These techniques are therefore potent to probe the electronic and local structure of the active material with surface modification under battery operating condition.¹⁹

This study aims on a comprehensive understanding of the surface coating mechanism. In our previous report, MgO coating on LiCoO₂ forms a solid solution phase at the LiCoO₂ surface, which occurs upon MgO coating at high temperatures.²⁰ However, different morphologies of MgO coating layer have been reported by other research group.^{6,21-24} In order to examine the morphology effect, we prepared two types of MgO coated-LiCoO₂ thin film electrodes at room temperature and high temperature. The stability at high potential cycling was investigated by electrochemical measurements. The electronic and local structural changes under battery operating conditions were tracked via *operando* TRF-XAS and DR-XAS measurements. By using these data, the surface coating mechanism is discussed from the view point of electronic and local structure at the electrode/electrolyte interface.

2. Experimental Methods

LiCoO₂ thin films were prepared on mirror-polished platinum substrates by pulsed laser deposition (PLD). Dense LiCoO₂ target with 15wt% excess Li₂O was used to compensate for Li loss during the deposition. A Nd:YAG laser ($\lambda = 266$ nm, 10 Hz repetition rate, 200 mW of power) was used. Deposition time, oxygen partial pressure and substrate temperature were 30 min, 0.01 Pa and 600°C, respectively. After the deposition of LiCoO₂, MgO was deposited onto the LiCoO₂ films by PLD for 30 s at room temperature or 60 s at 700°C. Hereafter, the uncoated LiCoO₂ thin film, the MgO coated LiCoO₂ thin films at room temperature and the films coated at 700°C are denoted as uncoated-LCO, RT-MgO-LCO and HT-MgO-LCO, respectively.

The as-prepared thin films were characterized by X-ray diffraction (XRD) and transmission electron microscopy (TEM) complemented with energy dispersive X-ray spectroscopy (EDX). Electrochemical measurements were performed using three-electrode cells. The working electrodes were the as-prepared thin films. The counter and reference

electrodes were lithium metal foils. A 1 M LiClO₄ in propylene carbonate was used as the electrolyte. Cyclic voltammetry was performed in the potential ranges of 3.2 V – 4.2 V, 3.2 V – 4.3 V, and 3.2 V – 4.4 V (*vs.* Li⁺/Li) with a sweep rate of 0.1 mV s⁻¹. Electrochemical impedance spectroscopy measurements were performed at frequencies that ranged from 10⁵ to 10⁻² Hz.

TRF-XAS measurements were performed on the beamlines BL01B1 and BL28XU of SPring-8 (Japan) using a solid-state detector. DR-XAS measurements were conducted at the beamline BL37XU of SPring-8 with a two-dimensional pixel array detector, PILATUS (Dectris, Switzerland). Co *K*-edge fluorescence XAS spectra were measured. For both *operando* XAS measurements, the customized spectro-electrochemical cells used consisted of the LiCoO₂ thin films as the working electrodes, lithium metal as the counter electrodes and 1 M LiClO₄ dissolved in a mixture of ethylene carbonate and diethyl carbonate with a volume ratio of 1:1 as the electrolyte. Experimental details of the *operando* DR-XAS and TRF-XAS measurements have been described elsewhere.^{15,17}

3. Results and Discussion

3.1 Characterization of as-prepared thin films

The as-prepared thin film electrodes were characterized by XRD, cross-sectional TEM as shown in Fig. 1. Except the diffraction peaks arising from Pt substrate, a peak at approximately $2\theta = 18.9^\circ$ is observed. This peak corresponds to diffraction by the (003) plane of hexagonal LiCoO₂. No other diffraction peaks were detected, validating the obtained LiCoO₂ film as a single phase oriented along the *c*-axis. The position of the diffraction peaks for the three thin films is almost equal, which indicates the bulk-crystal structure is unchanged upon MgO coating. The *c*-axis of the prepared LiCoO₂ film is tilted and not perpendicular to the substrate and the in-plane is random, meaning that the planes through which lithium ions

can intercalate in LiCoO_2 face the interface.¹⁵ The surface morphology measured by cross-sectional TEM with EDX of the RT-MgO-LCO is shown in Fig. 1(b). The EDX scan detected a Mg containing layer of approximately 5 nm in thickness outside Co containing layer for the RT-MgO-LCO. While the HT-MgO-LCO has a Mg layer within the LiCoO_2 surface²⁰, a Mg layer covers the surface of LiCoO_2 for the RT-MgO-LCO at the initial state.

3.2 Electrochemical properties of MgO coated LiCoO_2 thin films

The MgO coating on LiCoO_2 improves the durability especially at high potentials. Figure 2 shows the cyclic voltammograms (CVs) of uncoated-LCO, RT-MgO-LCO and HT-MgO-LCO at various upper limit potentials. The main peak observed at approximately 3.9 V is attributed to the first order phase transition between two hexagonal LiCoO_2 phases.²⁵ Two small peaks are observed at around 4.1 V and 4.15 V, which indicates that phase transitions occurs during lithium deintercalation.²⁵ When these three thin films are cycled below 4.2 V, the shapes of the CVs show good reversibility. The peak separation is small for the uncoated-LCO and the HT-MgO-LCO, while a clear separation is observed for the RT-MgO-LCO. When the potential range is increased, the cathodic peak diminishes drastically for the uncoated-LCO as shown in Figs. 2 (b) and 2 (c). On the other hand, this decrement is suppressed for the RT-MgO-LCO and HT-MgO-LCO even after charging to 4.4 V. The relationship between the coulombic efficiency calculated from the CVs and the upper limit potential is shown in Fig. 2 (d). The coulombic efficiency of the uncoated-LCO decreased drastically to less than 60 % after charging to 4.4 V. This irreversible reaction is suppressed for the RT-MgO-LCO and the HT-MgO-LCO. These results indicate that bare LiCoO_2 is easily deteriorated at high potentials and this degradation can be suppressed through MgO coating.

The effect of MgO coating is revealed by the resistance of the interfacial reaction via electrochemical impedance spectroscopy (EIS). Figure 3(a) shows typical Nyquist plots for EIS measured at various potentials. The observed main arcs correspond to the resistance of the interfacial reaction between the LiCoO₂ electrode and the electrolyte.²³ For the uncoated-LCO, the small arc observed at 4.0 V is drastically enlarged at 4.4 V. This result indicates that an inactive layer is formed on LiCoO₂ due to surface degradation.¹⁷ For the RT-MgO-LCO, the resistance is much greater than that of the uncoated-LCO at first. However the arc is not enlarged at 4.4 V but slightly diminishes. The interfacial resistances at each potential were estimated through the use of an equivalent circuit with the resistance in parallel with a constant-phase element (Fig. 3(b)). Both MgO coatings inhibit the increase of the interfacial resistance at 4.4 V as observed in the uncoated-LCO. The initial resistance of the RT-MgO-LCO is much larger than those of other films because the MgO layer deposited on the LiCoO₂ surface acts as a resistive phase. Interestingly, the resistance of RT-MgO-LCO increases from 4.0 V to 4.3 V, and then decreases from 4.3 V to 4.4 V in the charging process and the subsequent discharging processes. The reason behind this phenomenon will be discussed in the latter section.

3.3 Surface-sensitive *operando* XAS

To investigate the interfacial chemical structure on a nanometer scale, TRF-XAS measurements were performed for the three thin films. The information obtained from TRF-XAS mainly reflects the extreme interfacial structural features between electrodes and electrolytes under battery operating conditions.¹⁵ Figure 4(a) shows surface-sensitive X-ray absorption near edge structure (XANES) spectra at the Co *K*-edge measured via TRF-XAS of the prepared electrodes upon electrolyte immersion. In general, the absorption edge energy of XANES corresponds to the average valence of Co ions. For the uncoated-LCO, the absorption edge of XANES spectrum is located at lower energy than that of the RT-MgO-LCO and the

HT-MgO-LCO. The reduction behavior of Co ions for the uncoated-LCO immediately upon electrolyte immersion has been reported to be due to the reductive nature of organic electrolytes.¹⁵ The reduction of Co ions caused by electrolyte contact is suppressed by MgO coating as shown in Fig. 4(a). The energy at a normalized intensity of 0.5 of the XANES spectra (E_0) is plotted in Fig. 4(b) as a function of the various states of charge/discharge for the three thin films. For the uncoated-LCO, E_0 decreases immediately after electrolyte soaking and changes irreversibly during cycling between 3.8 V and 4.2 V. On the other hand, E_0 of the RT-MgO-LCO and the HT-MgO-LCO show reversible valence change. These results indicate that the MgO coating enhances the stability of the surface structure under battery operating condition.

3.4 Depth-resolved analysis of local structure change

Local structural changes of LiCoO_2 can be induced by the MgO coating and lithium extraction/insertion, especially around the electrode/electrolyte interface. The three thin films were investigated via DR-XAS, which can provide local structural information with a depth resolution of 3-4 nm.¹⁷ While the spectra collected at low-exit angles consist of signals only from the surface of the LiCoO_2 electrode due to self-absorption of fluorescence X-ray from deeper range, the spectra collected at high-exit angles include signals from both the surface and bulk. Local structural parameters, such as the interatomic distances and the Debye-Waller (DW) factors for the Co-O bonds were calculated by EXAFS analysis. DW factor reflects static local distortions for the Co-O bonds. The calculated Co-O length and the DW factor for the Co-O bonds at various states of charge are plotted as a function of the exit angles in Fig. 5. For this EXAFS analysis, the standard error of the Co-O length is less than 0.001 nm, and that of the Co-O DW factor is less than 0.002 nm. Although depth-resolved EXAFS analysis provides relatively large standard errors, one can discuss tendencies of the Co-O length and DW factor from the surface to the bulk as previously reported.^{17,18}

The temperature of MgO coating influences the surface structure of LiCoO₂. The Co–O length for the HT-MgO-LCO is longer than those of the other two thin films and is larger for low exit angles as shown in Fig. 5(a). The DW factor of the HT-MgO-LCO is larger than those for the others as shown in Fig. 5(d). This result can be explained by the formation of solid solution phase at LiCoO₂ surface as reported previously.²⁰ On the other hand, the Co-O length and the DW factor of the RT-MgO-LCO are almost similar to those of the uncoated-LCO. This result indicates that MgO layer only covers the LiCoO₂ surface and does not affect the local structure of LiCoO₂. The covered MgO layer for the RT-MgO-LCO impedes the interfacial reaction as observed in EIS measurement (Fig. 2).

Electrochemical lithium extraction causes rearrangement of local structure around the electrode/electrolyte interface. For the uncoated-LCO, when the cells are charged to 4.2 V, the DW factor at low exit angles increases (Fig. 6 (e)), meaning that structural distortion occurs at the interface.¹⁷ When the uncoated-LCO is charged to 4.4 V, the Co-O length at low angle is almost similar to the value observed at 4.2 V. The DW factor of the uncoated-LCO also increased at 4.4 V, particularly at the surface. These results show that the local structure of LiCoO₂ is deteriorated and the interfacial resistance is drastically increased.¹⁷ On the other hand, the parameter changes for the RT-MgO-LCO is similar to that of HT-MgO-LCO in which the Mg-containing solution layer in LiCoO₂ surface can stabilize the electrode/electrolyte interface at high potential.²⁰ When RT-MgO-LCO is charged, several Li⁺ sites become unoccupied, and Mg²⁺ ions at the surface can diffuse into the unoccupied Li⁺ sites. This process generates the solid solution phase of Mg at LiCoO₂ surface. Therefore the local structure of RT-MgO-LCO is similar to that of HT-MgO-LCO during charging process. The increase of the Co-O length and the DW factor observed in the uncoated-LCO at 4.4 V is inhibited for both the RT-MgO-LCO and HT-MgO-LCO. Therefore, the solid solution by Mg plays an important role for suppressing the local structure deterioration.

3.5. Comprehensive model for surface coating mechanism

In this section, we summarize the surface coating mechanism based on the experimental results. For the MgO coating, our results show two types of configuration. The first is MgO layer covering the LiCoO₂ surface as observed for the RT-MgO-LCO. The second is a solid solution formation at LiCoO₂ surface as observed for the HT-MgO-LCO. At the initial state, the former configuration influences the interfacial resistance, whereby the MgO layer covering LiCoO₂ impedes the interfacial reaction. However, the initial deterioration observed in the uncoated-LCO can be suppressed for both cases. A schematic illustration of the electrode/electrolyte interface for the examined three model thin films is shown in Fig. 6. Co reduction observed in the uncoated-LCO indicates that the electron transfer from the electrolyte to the surface forms the space charge layer at the LiCoO₂ surface.¹⁶ LiCoO₂ is reported to be a semiconductor with a relatively small band gap of ~1.5 eV.²⁶ Electrons from the electrolyte can move to the conduction band of the LiCoO₂. For the uncoated-LCO, the potential gap at the interface should be compensated by the space charge layer and the electrical double layer (Fig. 6 (a)).¹⁶ This wide space charge layer forms a Co-reduction phase. As shown in Fig. 2 (a), the phase transition of LiCoO₂ occurs at approximately 4.1 V. Although it has been reported that Mg-doping suppresses the phase transition and improves the stability of LiCoO₂,²⁷ the peak attributed to the phase transition was still observed for the RT-MgO-LCO and HT-MgO-LCO at approximately 4.1 V. This means that Mg-coating does not suppress the phase transition. Furthermore, the capacity degradation of the uncoated-LCO occurred through potential cycling between 3.2 V and 4.0 V. This supports that the surface structure change of the uncoated-LCO changes upon electrolyte immersion influences the charge-discharge stability.

In contrast, the MgO coating at room temperature inhibits the reduction of the Co ions at the LiCoO₂ surface upon electrolyte immersion. The band gap of MgO is much larger (6.4 eV)²⁸ than that of the LiCoO₂, preventing the electron transfer to the conduction band of the LiCoO₂. For RT-MgO-LCO, since the space charge layer does not form at the surface, the

potential gap between the electrode and the electrolyte is mostly compensated by the electrical double layer in the electrolyte (Fig. 6 (b)). In the case of HT-MgO-LCO, the solid-solution phase formed on the LiCoO₂ surface is very stable because the surface structure is not deteriorated even when the space charge layer forms at the electrode side (Fig. 6 (c)). Considering this, the suppression of the space charge layer formation in bare LiCoO₂ layer is an effective strategy to prevent initial deterioration of active materials during battery operation.

Control of the stability of the local structure in LiCoO₂ is also an important strategy. For the HT-MgO-LCO, the solid solution of Mg stabilizes the interfacial structure upon cycling at high potentials.²⁰ For the RT-MgO-LCO, the MgO layer only covers LiCoO₂ surface, leading to unfavorable increase in the interfacial resistance. However, as observed in the DR-XAS study, the local structure of the RT-MgO-LCO is similar to that of the HT-MgO-LCO during charging. When LiCoO₂ is charged, Li⁺ sites become unoccupied, and Mg²⁺ ions in the MgO can diffuse into the unoccupied Li⁺ sites because the ionic radius of Mg²⁺ is close to that of Li⁺ (Fig. 7).²⁹ Therefore a solid solution with Mg²⁺ serves as the pillar in layered structure of LiCoO₂ even in the RT-MgO-LCO during cycling. Hard X-ray photoemission spectra for the 2s state of Mg as a function of charge state were measured. The binding energy of Mg 2s of the HT-MgO-LCO is constant before and after charging. For the RT-MgO-LCO, the peak position at Mg 2s is shifted toward higher energy and attained the same value as that observed for HT-MgO-LCO. This result supports the formation of a solid-solution phase in RT-MgO-LCO following the charging reaction. Moreover, the interfacial resistance of the RT-MgO-LCO drastically decreases from 4.3 to 4.4 V and subsequent discharge processes. On the other hand, the order of magnitude of interfacial resistance in the HT-MgO-LCO is almost constant under potential cycling. These phenomena supports our explanation, which is Mg²⁺ initially covered on the RT-MgO-LCO diffuses into LiCoO₂ layer and the local structure of the RT-MgO-LCO approaches the HT-MgO-LCO. The formation of stabilized local structure at

the electrode/electrolyte interface with delithiated condition is the other strategy for enhancing of high potential operation.

4. Conclusion

The mechanism of the MgO coating on LiCoO₂ was investigated via electrochemical measurements and *in operando* XAS measurements. MgO coating at both room temperature and high temperature improves the durability under high-potential cycling. The initial deterioration caused by Co reduction of the uncoated-LiCoO₂ thin films is inhibited by MgO coating. For the MgO coating conducted at high temperature, a solid solution phase is formed on LiCoO₂ surface which stabilizes the delithiated layered structure. For the MgO coating conducted at room temperature, the MgO layer only covers the surface of LiCoO₂ at the initial state. During the charge process, Mg²⁺ ions at the surface diffuse into the unoccupied Li⁺ sites of LiCoO₂. In both cases, Mg ions serve as pillars in LiCoO₂ layer to improve the stability at high potential.

Acknowledgements

This work was partially supported by the “Research and Development Initiative for Scientific Innovation of New Generation Battery (RISING project)” of the New Energy and Industrial Technology Development Organization (NEDO), Japan. The synchrotron radiation experiments were performed with approval from the Japan Synchrotron Radiation Research Institute (JASRI) (Proposal Nos. 2009B1027, 2010A1015, 2010A1016, 2010B1029, 2011A1012, 2011B1022, 2011B1023, and 2011B1037).

Reference

- [1] K. Xu, and A. von Cresce, *J. Mater. Chem.*, **21**, 9849 (2011).

- [2] Z. Chen, Y. Qin, K. Amine, and Y. K. Sun, *J. Mater. Chem.*, **20**, 7606 (2010).
- [3] S.-T. Myung, K. Amine, and Y.-K. Sun, *J. Mater. Chem.*, **20**, 7074 (2010).
- [4] M. Shikano, H. Kobayashi, S. Koike, H. Sakaebe, E. Ikenaga, K. Kobayashi, and K. Tatsumi, *J. Power Sources*, **174**, 795 (2007).
- [5] H. Miyashiro, A. Yamanaka, M. Tabuchi, S. Seki, M. Nakayama, Y. Ohno, Y. Kobayashi, Y. Mita, A. Usami, and M. Wakihara, *J. Electrochem. Soc.*, **153**, A348 (2006).
- [6] Y. Gu, D. Chen, X. Jiao, and F. Liu, *J. Mater. Chem.*, **17**, 1769 (2007).
- [7] J. Zhao, and Y. Wang, *J. Phys. Chem. C*, **116**, 11867 (2012).
- [8] S.-T. Myung, K. Izumi, S. Komaba, Y.-K. Sun, H. Yashiro, and N. Kumagai, *Chem. Mater.*, **17**, 3695 (2005).
- [9] J. Liu, and A. Manthiram, *Chem. Mater.*, **21**, 1695 (2009).
- [10] Z. Chen, and J. R. Dahn, *Electrochem. Solid-State Lett.*, **5**, A213 (2002).
- [11] S. Verdier, L. El Ouatani, R. Dedryvère, F. Bonhomme, P. Biensan, and D. Gonbeau, *J. Electrochem. Soc.*, **154**, A1088 (2007).
- [12] I. D. Scott, Y. S. Jung, A. S. Cavanagh, Y. Yan, A. C. Dillon, S. M. George, and S.-H. Lee, *Nano Lett.*, **11**, 414 (2011).
- [13] K. Sakamoto, M. Hirayama, N. Sonoyama, D. Mori, A. Yamada, K. Tamura, J. Mizuki, and R. Kanno, *Chem. Mater.*, **21**, 2632 (2009).
- [14] M. Hirayama, N. Sonoyama, T. Abe, M. Minoura, M. Ito, D. Mori, A. Yamada, R. Kanno, T. Terashima, M. Takano, K. Tamura and J. Mizuki, *J. Power Sources*, **168**, 493 (2007).
- [15] D. Takamatsu, Y. Koyama, Y. Orikasa, S. Mori, T. Nakatsutsumi, T. Hirano, H. Tanida, H. Arai, Y. Uchimoto, and Z. Ogumi, *Angew. Chem., Int. Ed.*, **51**, 11597 (2012).
- [16] K. Yamamoto, T. Minato, S. Mori, D. Takamatsu, Y. Orikasa, H. Tanida, K. Nakanishi, H. Murayama, T. Masese, T. Mori, H. Arai, Y. Koyama, Z. Ogumi, and Y. Uchimoto, *J. Phys. Chem. C*, **118**, 9538 (2014).
- [17] D. Takamatsu, T. Nakatsutsumi, S. Mori, Y. Orikasa, M. Mogi, H. Yamashige, K. Sato, T. Fujimoto, Y. Takanashi, H. Murayama, M. Oishi, H. Tanida, T. Uruga, H. Arai, Y. Uchimoto and Z. Ogumi, *J. Phys. Chem. Lett.*, **2**, 2511 (2011).
- [18] T. Okumura, T. Nakatsutsumi, T. Ina, Y. Orikasa, H. Arai, T. Fukutsuka, Y. Iriyama, T. Uruga, H. Tanida, Y. Uchimoto and Z. Ogumi, *J. Mater. Chem.*, **21**, 10051 (2011).
- [19] D. Takamatsu, S. Mori, Y. Orikasa, T. Nakatsutsumi, Y. Koyama, H. Tanida, H. Arai, Y. Uchimoto, and Z. Ogumi, *J. Electrochem. Soc.*, **160**, A3054 (2013).
- [20] Y. Orikasa, D. Takamatsu, K. Yamamoto, Y. Koyama, S. Mori, T. Masese, T. Mori, T. Minato, H. Tanida, T. Uruga, H. Arai, Z. Ogumi, and Y. Uchimoto, *submitted for publication*.
- [21] Z. Wang, C. Wu, L. Liu, F. Wu, L. Chen, and X. Huang, *J. Electrochem. Soc.*, **149**, A466 (2002).

- [22] Z. Wang, X. Huang, and L. Chen, *J. Electrochem. Soc.*, **150**, A199 (2003).
- [23] Y. Iriyama, H. Kurita, I. Yamada, T. Abe, and Z. Ogumi, *J. Power Sources*, **137**, 111 (2004).
- [24] H. Zhao, L. Gao, W. Qiu, and X. Zhang, *J. Power Sources*, **132**, 195 (2004).
- [25] J. N. Reimers, and J. R. Dahn, *J. Electrochem. Soc.*, **139**, 2091 (1992).
- [26] A. Juhin, F. De Groot, G. Vankó, M. Calandra, and C. Brouder, *Phys. Rev. B*, **81**, 115115 (2010).
- [27] S. Levasseur, M. Menetrier, and C. Delmas, *J. Power Sources*, **112**, 419 (2002).
- [28] J. A. McLeod, R. G. Wilks, N. A. Skorikov, L. D. Finkelstein, M. Abu-Samak, E. Z. Kurmaev, and A. Moewes, *Phys. Rev. B*, **81**, 245123 (2010).
- [29] R. D. Shannon, *Acta Cryst.*, **A32**, 751 (1976).

Fig. 1. (a) XRD spectra of the uncoated-LCO, the RT-MgO-LCO and HT-MgO-LCO on Pt substrates. Only the diffraction peak at 18.9° is observed, except for the diffraction peak from the Pt substrate. Diffraction peaks from MgO are not observed due to the exceedingly low amount of MgO. (b) Micrographs from cross-sectional dark-field transmission electron microscopy (left) and results from energy-dispersive X-ray (EDX) line scans (right) of the RT-MgO-LCO.

Fig. 2. Cyclic voltammograms of the uncoated-LCO, the RT-MgO-LCO and HT-MgO-LCO between (a) 3.2 V-4.2 V, (b) 3.2 V-4.3 V and (c) 3.2 V-4.4 V and (d) the coulombic efficiency of these electrodes obtained from (a)-(c).

Fig. 3. (a) Nyquist plots of the uncoated-LCO and the RT-MgO-LCO at 4.0 V and 4.4 V. (b) Interfacial resistance estimated via EIS of the uncoated-LCO, RT-MgO-LCO and HT-MgO-LCO as a function of the potentials. For the uncoated-LCO at 4.4 V, the interfacial resistance cannot be calculated because the Nyquist plots are similar to those for blocking electrodes.

Fig. 4. (a) XANES from *operando* TRF-XAS measurements of the uncoated-LCO, the RT-MgO-LCO and the HT-MgO-LCO after electrolyte immersion. (b) Shift in the absorption energy at normalized intensity of 0.5 (E_0) measured with TRF-XAS under battery operating condition.

Fig. 5. The dependence of (a)-(c) the Co-O interatomic distance and (d)-(f) the Co-O DW factor on the exit angles of the uncoated-LCO, RT-MgO-LCO and HT-MgO-LCO obtained from *operando* DR-XAS. (a) and (d) were measured prior to charging. (b) and (e) were measured

after charged up to 4.2 V. (c) and (f) were measured after charged up to 4.4 V. Low exit angles indicate positions closer to the surface. Co-O interatomic distance and Co-O DW factor obtained at low exit angles reflect on information about the surface of a thin film, whereas obtained at high exit angles reflect on more information about the bulk property.

Fig. 6. Schematic view of the surface coating effect on the LiCoO₂ surface. The electronic structure at (a) the uncoated-LCO/electrolyte interface, (b) the RT-MgO-LCO/electrolyte interface and (c) the HT-MgO-LCO/electrolyte interface upon electrolyte immersion. (ϕ_S and ϕ_L are the electrochemical potentials of the electrode and electrolyte, respectively).

Fig. 7. Schematic view of the Mg²⁺ diffusion into unoccupied Li⁺ sites at the RT-MgO-LCO surface. Prior to charging (left), MgO layer just covers the LiCoO₂ surface. After charging (right), unoccupied Li sites generate in the LiCoO₂ and Mg²⁺ in the MgO diffuses to the unoccupied Li sites.

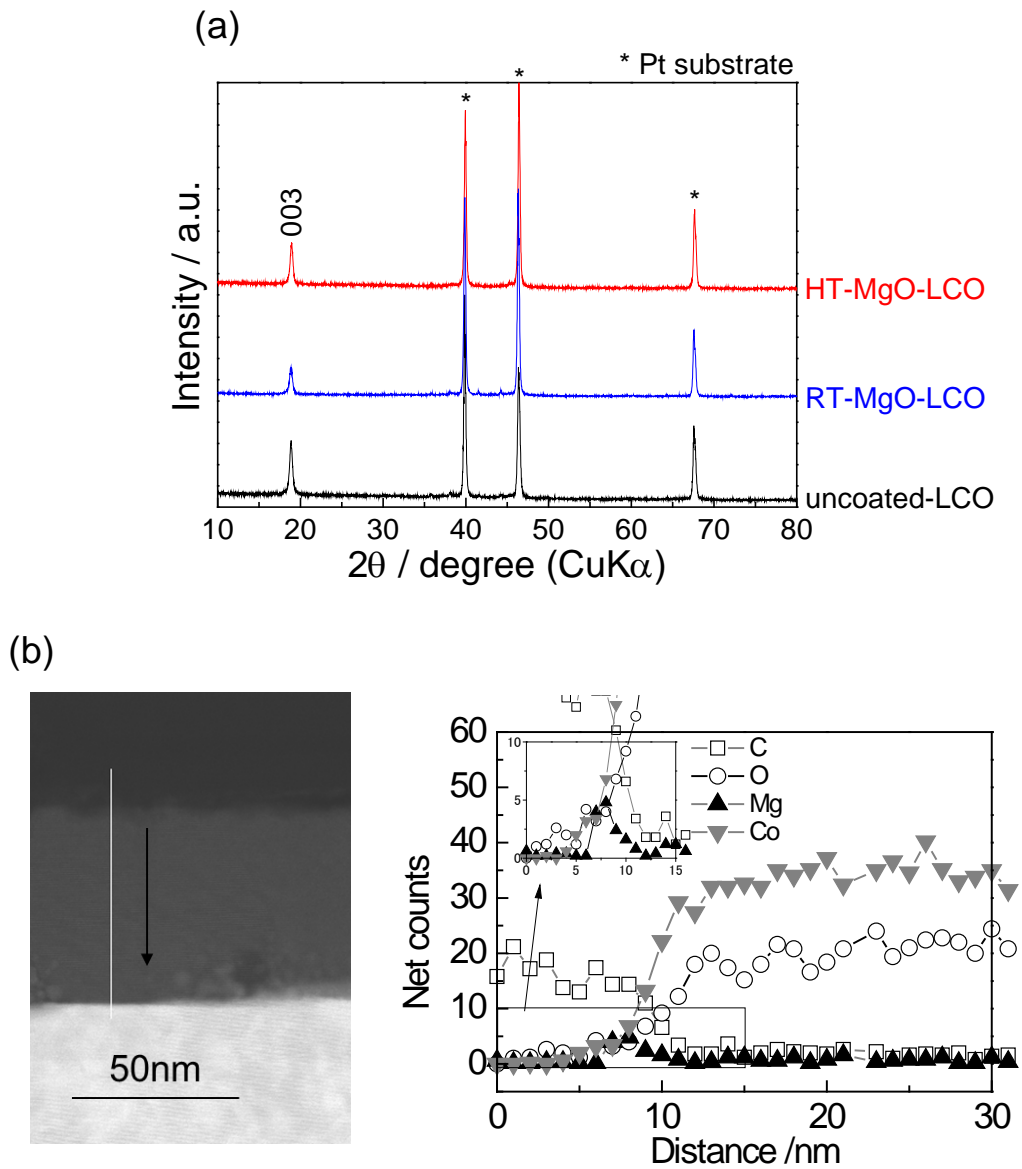


Fig. 1 Yamamoto *et al.*

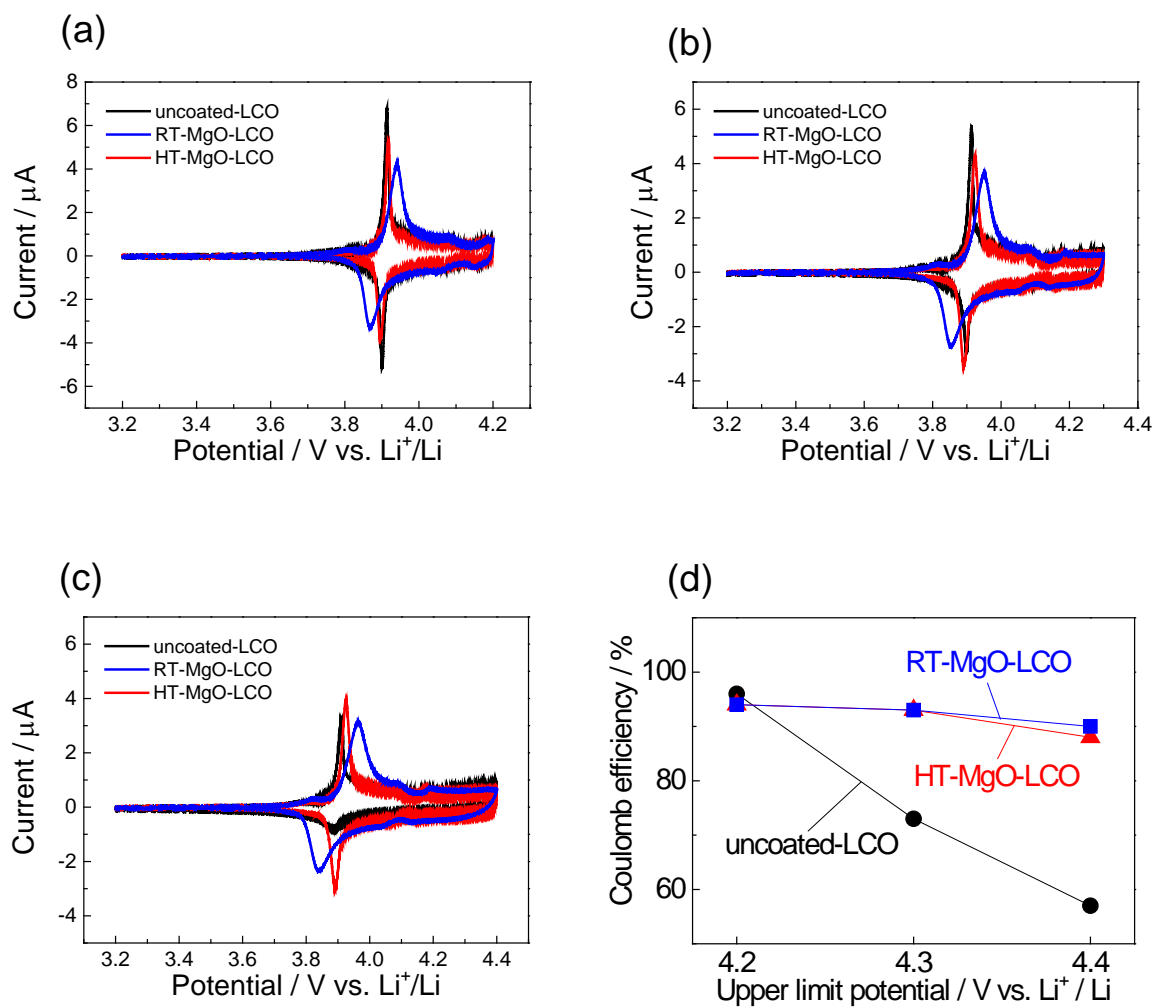


Fig. 2 Yamamoto *et al.*

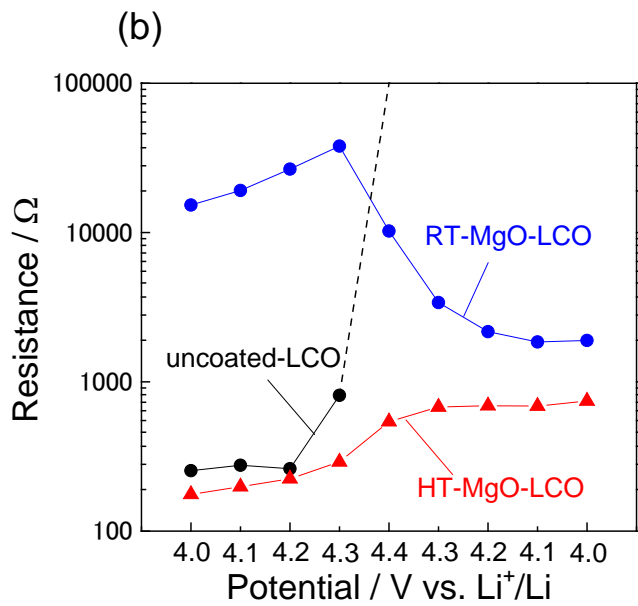
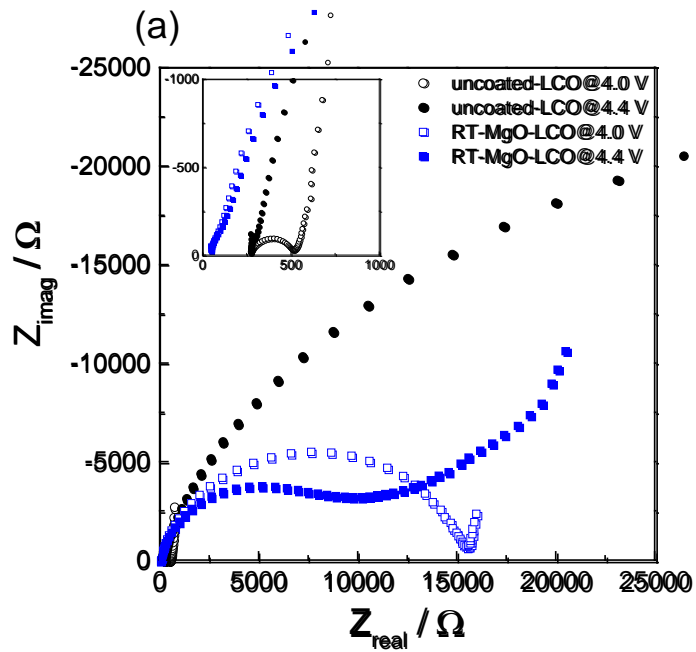


Fig. 3 Yamamoto *et al.*

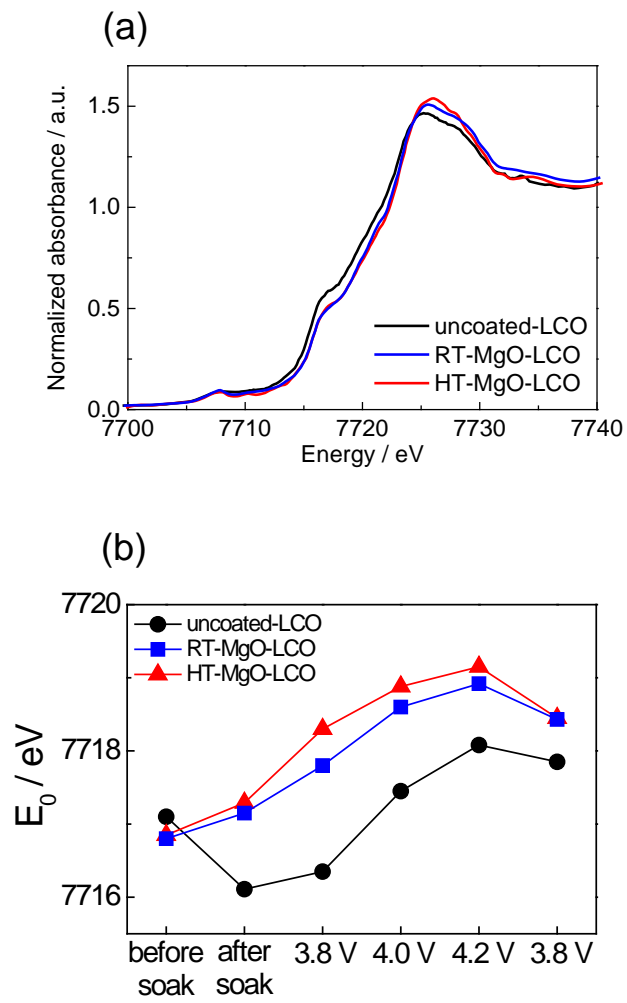


Fig. 4 Yamamoto *et al.*

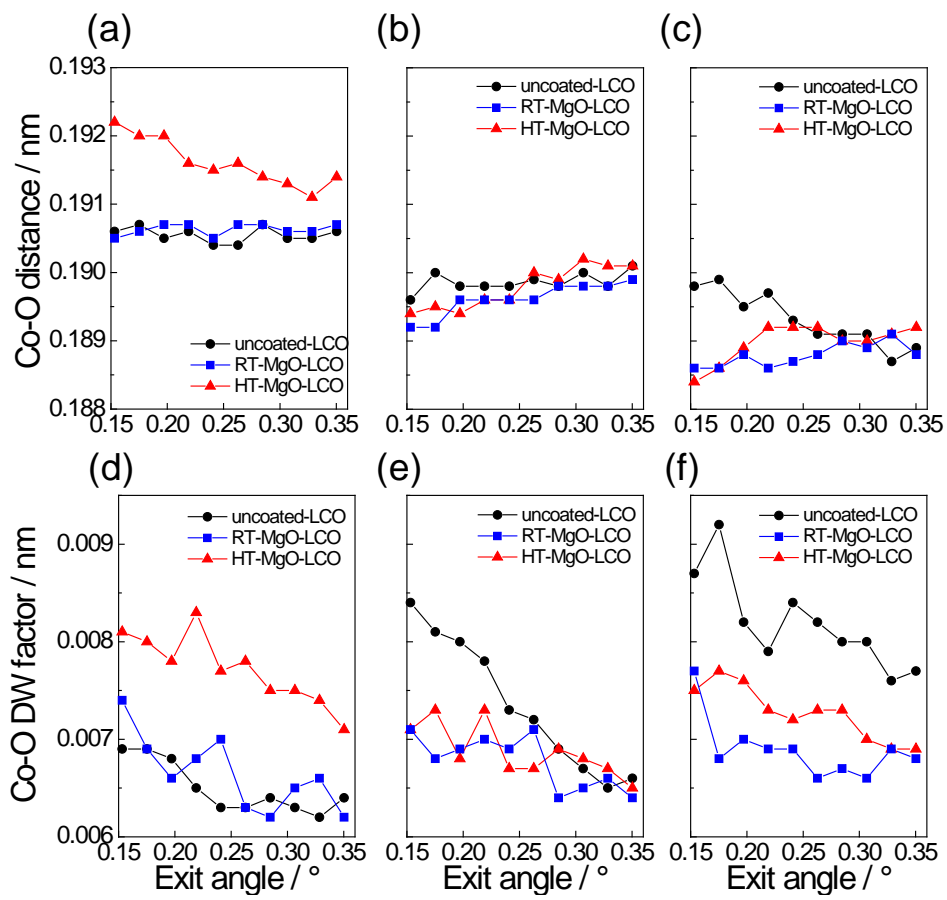


Fig. 5 Yamamoto *et al.*

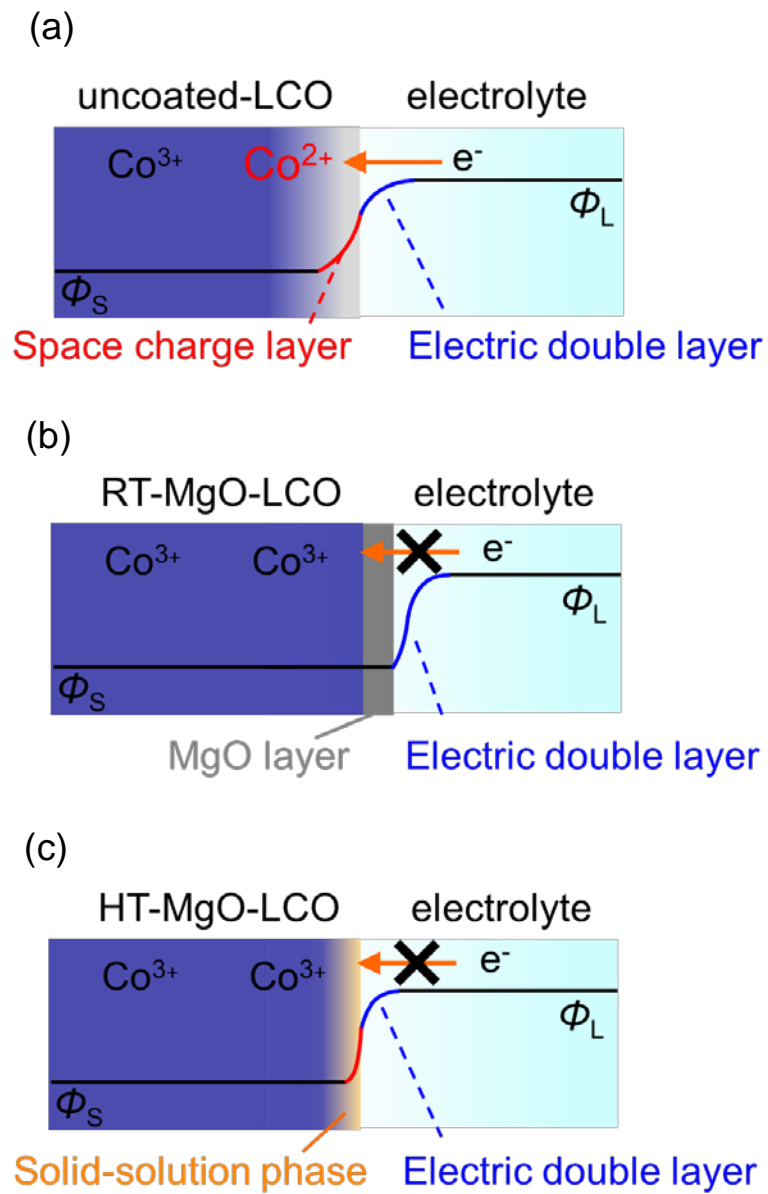


Fig. 6 Yamamoto *et al.*

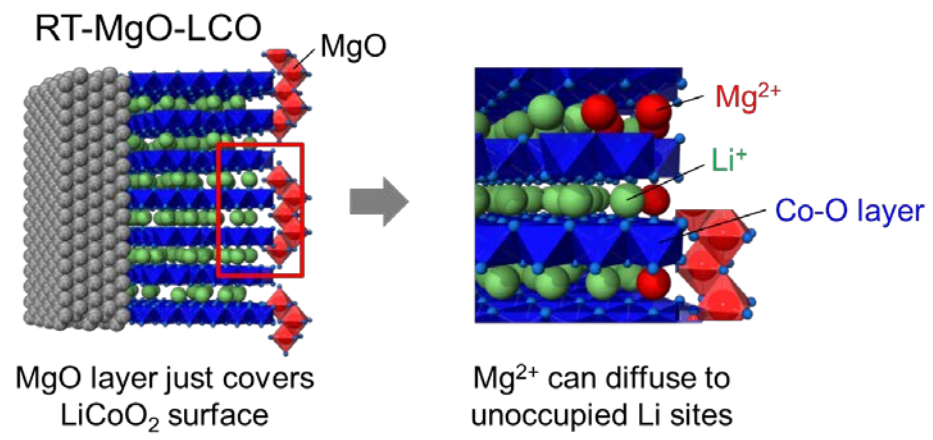


Fig. 7 Yamamoto *et al.*